Applied Surface Science 687 (2025) 162305

Contents lists available at ScienceDirect

Applied Surface Science

journal homepage: www.elsevier.com/locate/apsusc

Full Length Article

Short-range order and memory properties of silicon oxide –based memristors

G.N. Kamaev [a,*], Yu.N. Novikov [a], I.P. Prosvirin [b], A.A. Gismatulin [a], A.R. Khanas [c], A.V. Zenkevich [c], V.A. Gritsenko [a,d]

[a] Rzhanov Institute of Semiconductor Physics SB RAS, 13 Lavrentiev Aven., Novosibirsk 630090, Russia
[b] Boreskov Institute of Catalysis SB RAS, 5 Lavrentiev aven., Novosibirsk 630090, Russia
[c] Moscow Institute of Physics and Technology, Moscow Region, Dolgoprudny 141701, Russia
[d] Novosibirsk State Technical University, 20 Marx Aven, Novosibirsk 630073, Russia

ARTICLE INFO

Keywords:
Memristor
Resistive switching
Silicon oxide
X-ray photoelectron spectroscopy
Short-range order

ABSTRACT

The relation between the structure of amorphous SiO_x films of various compositions obtained by plasma-enhanced chemical vapor deposition and the characteristics of Resistive Random-Access Memory (ReRAM) devices with the active layer based on such films were investigated. The composition of the samples was studied using X-ray photoelectron spectroscopy. A comparison of the experimental Si 2p photoelectron spectrum with calculations showed that the short-range order in the arrangement of atoms in the amorphous SiO_x films is defined by the content of excess silicon and can be described within the framework of different structural models. The short-range order has a decisive influence on the memristor characteristics of obtained films. Memristors based on SiO_x whose active layer obeys the Random Bonding model exhibit a more pronounced hysteresis window and high stability of the resistive switching of ReRAM devices between two stable (low- and high-resistive) states.

1. Introduction

Resistive random-access memory (ReRAM) is emerging as a potential substitute of flash memory due to its high speed, long data storage time, lower energy consumption and simple manufacturing processes featuring a good scalability of fabricated devices. Memristors that have multiple intermediate states or operate in analog mode are capable of modeling brain synapses. Such synaptic memristor networks are also capable of learning and adaptive computing [1–9].

Developing memristors with an active layer based on materials that are fully compatible with the modern CMOS technology is an important though challenging problem. In this respect, silicon-based dielectrics (SiO_x, SiN_x, and SiO_xN_y) are of great interest [10–19]. However, ReRAM programming currents are normally higher than those required for creating the next-generation non-volatile memory (NVM). For this reason, reducing the current and power consumption in the memristors of interest is an important issue for the use of ReRAM in various applications [20].

One approach to solving this problem is the reduction of the memristor current in the high-resistive state (HRS) [21,22]. As a rule, this current defines the memristor memory window (the ratio of the currents in the on– and off-states (ON\OFF)). In the publications [15,22], it was shown that the on-current can be decreased by reducing the content of excess silicon in the film. However, a simple change in the ratio between the contents of Si and O_2\N_2 in the active-layer material based on a non-stoichiometric silicon-containing dielectric does not always lead to the ability to control the efficiency of ReRAM devices. The stoichiometry of the active layer is not the only factor affecting ReRAM characteristics since SiO_x, SiN_y and SiO_xN_y films with the same composition may possess different structure [23,24]. For instance, I.P. Lisovskyy *et al.* [23] have studied the separation of phases in non-stoichiometric SiO_x films during high-temperature annealing. They observed the evolution of Si2p core-level spectrum in XPS for the films with $x = 1.6$ following the increase of the annealing temperature and the appearance of two characteristic peaks in the spectra corresponding to Si and SiO_2. The Si 2p spectra demonstrated a monotonic increase of the Si^0 component intensity upon annealing in the temperature range from 700 to 1100 °C. The effect of the chemical composition and the

* Corresponding author.
E-mail addresses: kamaev@isp.nsc.ru (G.N. Kamaev), aagismatulin@isp.nsc.ru (A.A. Gismatulin), grits@isp.nsc.ru (V.A. Gritsenko).

https://doi.org/10.1016/j.apsusc.2025.162305
Received 16 September 2024; Received in revised form 26 December 2024; Accepted 2 January 2025
Available online 3 January 2025
0169-4332/© 2025 Elsevier B.V. All rights are reserved, including those for text and data mining, AI training, and similar technologies.

microstructure of thin amorphous hydrogenated silicon nitride films enriched in silicon on their photoluminescence properties was investigated in [24]. For SiN_y films, two luminescence mechanisms were identified depending on the annealing temperature. These mechanisms are defined not only by the composition of the dielectric, but also by the short-range order in the arrangement of atoms. At annealing temperatures above 800 °C a phase separation occurs, and the films can be described as an amorphous silicon nitride matrix with embedded silicon nanoclusters.

Thus, silicon-based dielectric layers of identical non-stoichiometric composition may have different structures, or short-range order, in the arrangement of atoms. It is therefore important to take into account the effect of the short-range order on the physical properties of the dielectric. In particular, it was previously shown [25] that ReRAM devices with an active SiO_xN_y layer with the structure described using the Random Bonding model, have a maximum memory window. For this reason, it is of both scientific and practical interest to study the influence of the short-range atomic order in non-stoichiometric SiO_x layers of various compositions in memristor devices on their functional characteristics.

2. Experiments

SiO_x films of various compositions were grown by plasma-enhanced chemical vapor deposition (PECVD) technique from a gas mixture of monosilane and oxygen in the facility with remote plasma inductively excited by a generator at 13.56-MH frequency. The rate of the monosilane flow supplied to the reaction zone (a gas mixture of 10 % of SiH_4 diluted with Ar) was fixed at 10 cm^3/min. The composition of SiO_x was varied by changing the rate of oxygen flow in the gas mixture. The substrate temperature during the deposition was 200 °C. The RF oscillator power was 50 W. The SiO_x layers were deposited onto silicon substrates with the natural oxide etched out prior to deposition. The substrates used were p-type (100)-oriented Czochralski-grown boron doped single-crystal Si wafers with resistivity of ≈0.003 Ohm·cm. The composition of the SiO_x films was determined with X-ray photoelectron spectroscopy (XPS) using SPECS instrument ($h\nu$ = 1486,74 eV) by assessing the integral intensities of Si2p- and O1s peaks, taking into account the atomic sensitivity coefficients [25,26].

The description of the short-range order in the arrangement of atoms in the SiO_x layers was performed within the framework of three models [27–29]. According to the Random Bonding (RB) model, there are five types of Si-$O_\nu Si_{4-\nu}$ tetrahedra (where ν = 0, 1,…, 4) in the SiO_x layers with some oxygen atoms replaced by silicon. In the Random Mixture (RM) model, the non-stoichiometric SiO_x is a mixture of the SiO_2 phase (Si-O_4 tetrahedra) and the Si phase (Si-Si_4 tetrahedra). In the Intermediate model (IM) [28,29], the presence of five types of Si-$O_\nu Si_{4-\nu}$ tetrahedra is assumed; however, unlike the RB model, the statistic of those tetrahedra is not described by the binomial distribution. When analyzing the XPS spectra of Si2p from SiO_x in all the three cases, it is assumed that the main contribution to the spectrum comes from five Si-$O_\nu Si_{4-\nu}$ tetrahedra (where ν = 0, 1,…, 4) where a Si atom is located at the vertex. For the Si-Si_4 (Si) and Si-O_4 (SiO_2) tetrahedra, the following energy positions of the intensity peaks (and their half-widths) adopted in the calculations were: 99.35 eV (0.6 eV) and 103.52 eV (1.2 eV), respectively. The energy position and the half-width of the peaks due to Si-$O_\nu Si_{4-\nu}$ tetrahedra (where ν = 1, 2, 3) were determined based on the assumption of a linear dependence of both parameters on the number of O atoms in the tetrahedron. In the IM, the contributions due to the five Si-$O_\nu Si_{4-\nu}$ tetrahedra were chosen in order to achieve the best agreement with the experimental Si2p spectrum [28,29]. The results of calculations are given in Table 1.

To study the electrical properties of the films, metal–insulator-semiconductor (MIS) structures were fabricated, in which ~ 40 nm thick SiO_x films were used as an active memristor layer. The top nickel electrodes ~ 200 nm in thickness and sizes varying from 0.018 to 0.5 mm^2 were deposited by magnetron sputtering through a shadow mask. The highly doped silicon substrate served a bottom electrode. The current–voltage and endurance measurements were carried out on a Keysight B1500A setup. The method for measuring endurance consisted of applying write/erase pulses with read pulse only at checkpoints to accumulate a large number of switching cycles and save measuring time [30,31]. During the reading, the adaptive write/erase pulse tuning algorithm was also used [32,33]. Such a complex measurement algorithm is used to improve the variability and memristor endurance.

3. Results and discussion

Fig. 1a shows the experimental and calculated Si 2p XPS spectra in the SiO_x layer grown at the oxygen flow rate of 4 cm^3/min. The experimental Si 2p spectrum exhibits two peaks due to different phases of non-stoichiometric silicon oxide (Si^0 and Si^{4+}). In this case, the short-range order in SiO_x obeys the RM model. The calculated peak intensities fit the experimental peaks fairly well. From the analysis of the spectrum, it follows that the grown SiO_x layer has the composition $SiO_{1.12}$.

Fig. 1b shows the I-V characteristics of the memristor with an active $SiO_{1.12}$ layer measured during three cycles of bipolar switching from a high- to low-resistive state. However, with each subsequent cycle the memory window is seen to become smaller. The cycling measurements showed a complete degradation of the device following the first ten cycles.

Fig. 2a shows the experimental and calculated XPS spectra of Si 2p in a SiO_x layer deposited at the increased oxygen flow rate 7 cm^3/min. In contrast to the previous case, the only component is clearly observed in the experimental Si 2p spectrum, with no additional peak attributed to the Si-Si_4 tetrahedra. For the obtained SiO_x film, the calculations were performed within the framework of both RB and IM models, and the best agreement with the experimental Si 2p spectrum was observed for the case when the short-range order in the arrangement of atoms is described by the IM model (see Fig. 2a). From the analysis of XPS spectra it follows that the obtained SiO_x layer has the composition $SiO_{1.59}$.

Fig. 2b shows I-V characteristics and cycling data taken for the memristor device with the active $SiO_{1.59}$ layer. The bipolar switching is again observed as for $SiO_{1.12}$ layer, but the current in the low- and high-resistive states are more stable, and the memory window reaches more than two orders of magnitude. Nevertheless, after two dozen switching

Table 1
Results of calculations made using the RM, IM and RB models for various compositions of SiO_x active layers.

N	Binding energy, eV	Number of atoms at the base of the tetrahedron		$SiO_{1.12}$ (Fig. 1)	$SiO_{1.59}$ (Fig. 2)		$SiO_{1.82}$ (Fig. 3)
				RM Percentage of tetrahedra	RB Percentage of tetrahedra	IM Percentage of tetrahedra	RB Percentage of tetrahedra
		Si	O				
0	99.35	4	0	18	0.18	0	0
1	100.35	3	1	–	2.74	7.14	0
2	101.41	2	2	–	15.94	0	0.23
3	102.47	1	3	–	41.2	21.43	7.53
4	103.52	0	4	82	39.95	71.43	92.24

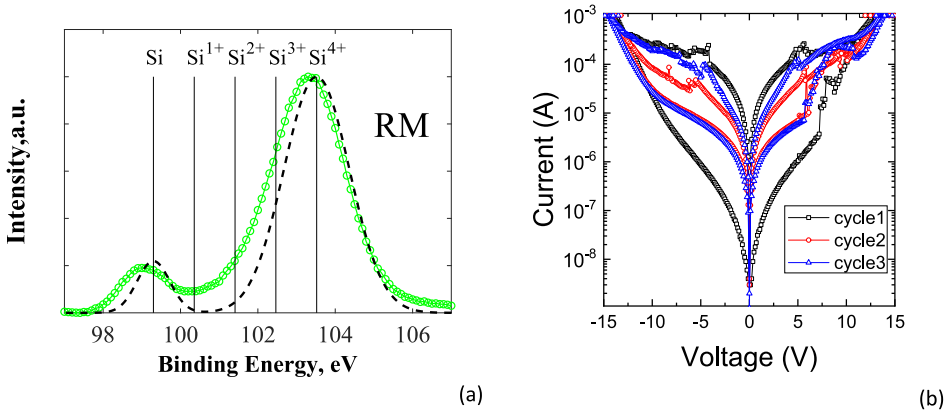

FIG. 1. (a) The comparison of the experimental Si 2p spectrum (green) with the one calculated by the RM model (dashed line) for $SiO_{1.12}$ and (b) the switching characteristics of the $SiO_{1.12}$ -based memristor with 0.5 mm^2 contact area.

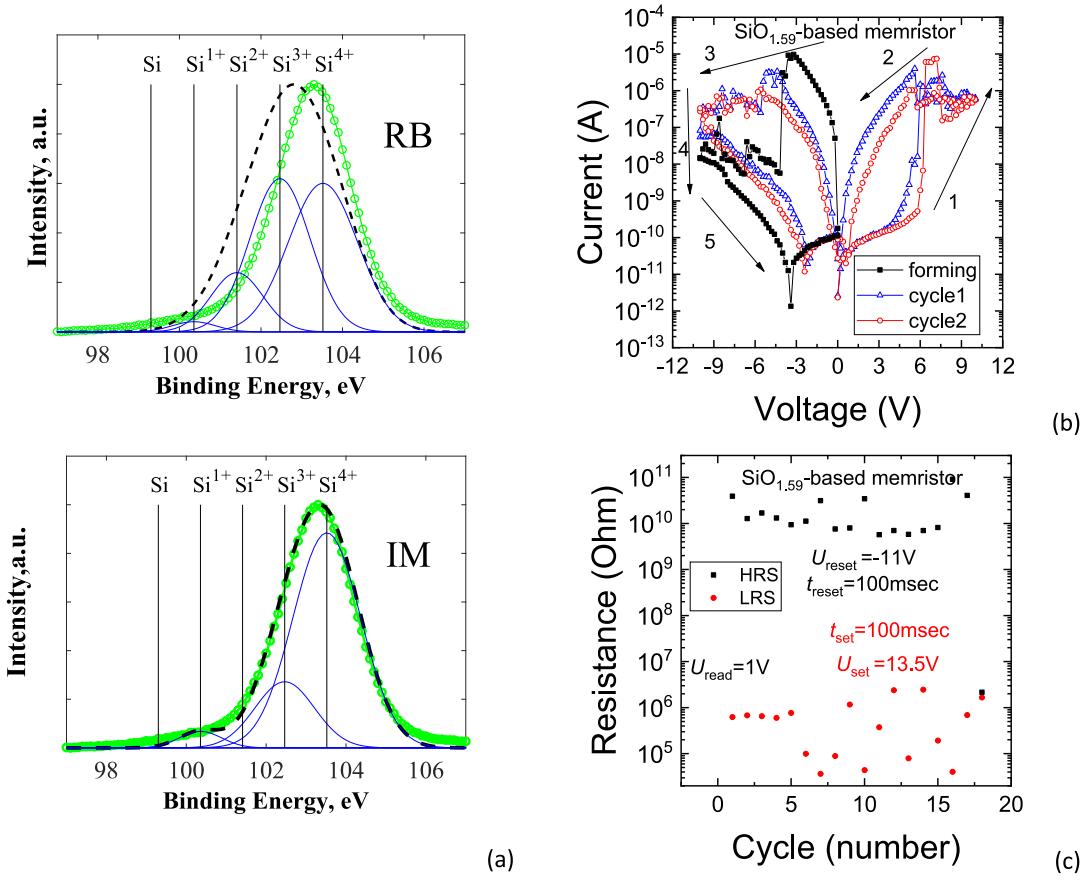

FIG. 2. (a) Comparison of the experimental Si 2p spectrum (green) with those calculated by the RB and IM models (dashed line) for $SiO_{1.59}$, (b) I-V characteristics of the $SiO_{1.59}$ -based memristor, and (c) its degradation upon cycling (0.018 mm^2 contact area).

cycles, the devices no longer display switching from the conducting state, thus pointing at their degradation (Fig. 2c).

Fig. 3a shows the experimental and calculated Si 2p spectra for SiO_x layer grown at the oxygen flow rate of 10 cm^3/min. The calculations were performed assuming the presence of a short-range order in the arrangement of atoms obeying the RB model. Both the experiment and calculation of the Si 2p spectrum demonstrate the presence of one peak observed at the BE = 103.5 eV. The modelled spectrum is in satisfactory agreement with the experimental one. According to the XPS data, the grown SiO_x layer here has the composition $SiO_{1.82}$.

The I-V characteristics taken from the memristor device employing $SiO_{1.82}$ active layer as well as the results of the endurance test are shown in Fig. 3b and c, respectively. The OFF/ON ratio is around 5, and it remains stable after 10^7 switching cycles, thus exhibiting a good durability of examined devices.

Let us perform a comparative analysis of the results shown in Figs. 1-3. The increasing of the oxygen flow rate gives rise to the substantial change in the observed XPS spectra. This means that the deposition mode of the SiO_x layer exert a profound influence on both the composition and short-range order in the arrangement of atoms in the dielectric. At the oxygen flow rate of 4 cm^3/min, the registered XPS spectra exhibit two distinct peaks pointing at the SiO_2 (103.52 eV) and Si (99.35

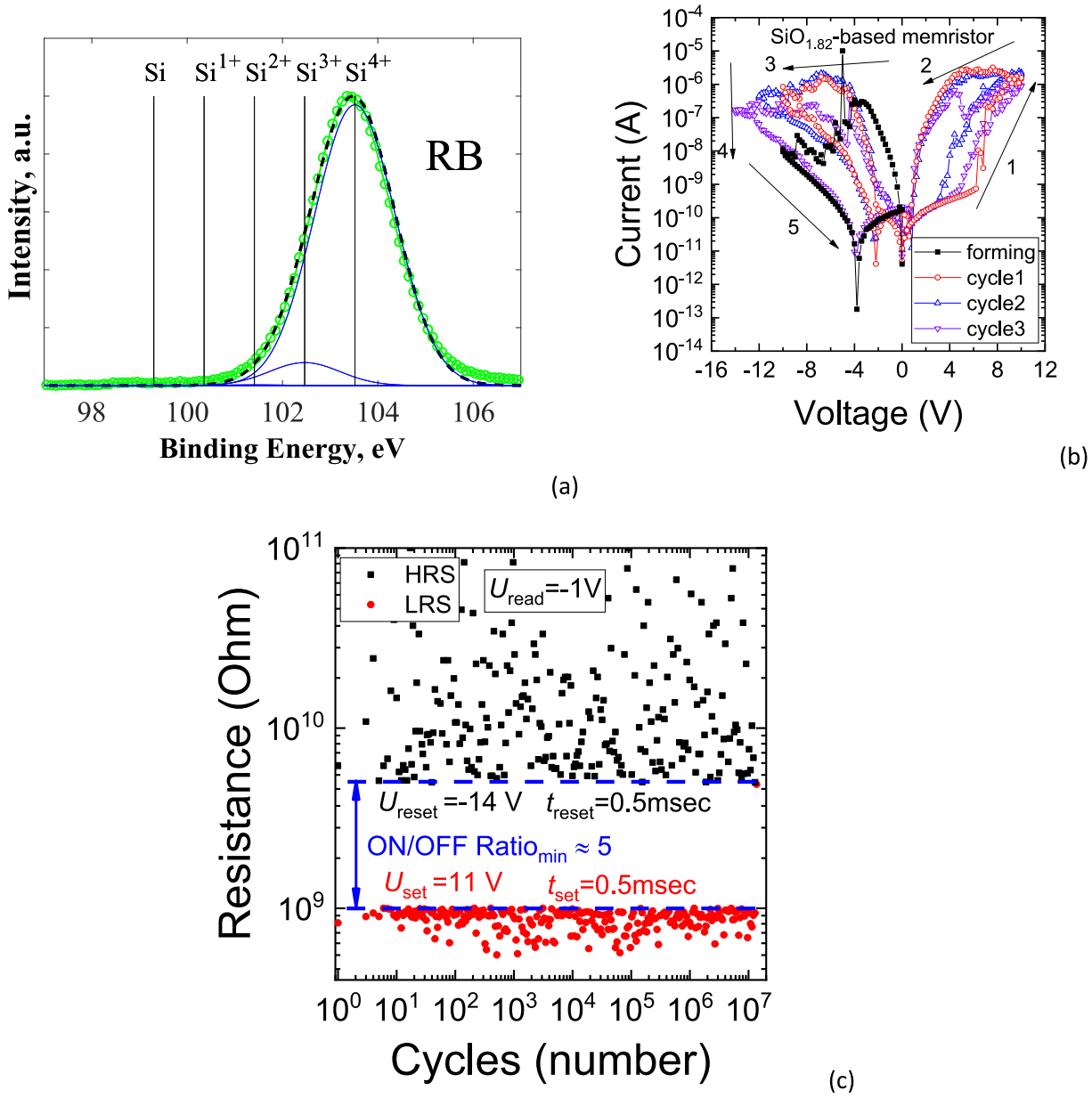

FIG. 3. (a) Comparison of the experimental Si 2p spectrum (green) with the one calculated with the RB model (dashed line) for $SiO_{1.82}$, (b) the I-V characteristics of the $SiO_{1.82}$ -based memristor, and (c) its endurance (0.018 mm^2 contact area).

eV) chemical bonding. The increasing of the oxygen content in the gas mixture results in the peak related to the Si^0 bonding (99.35 eV) becoming less pronounced (see Fig. 2a). In Fig. 3a, there is a single peak with the maximum observed at the 103.52 eV; this peak is related with the SiO_2 bonding. The analysis of the microstructure of amorphous SiO_x films shows that the short-range order in the arrangement of atoms in such films can be described within the framework of RM, intermediate, and RB models depending on the Si/O elemental composition.

Thus, we conclude that the short-range order in the arrangement of atoms in SiO_x films has the decisive role on the functional characteristics of memristor devices. In particular, the memristor devices based on SiO_x whose active layer obeys the RB model exhibit a larger hysteresis window, a more stable resistive switching behavior of the active layer, and a lower current in the OFF-state. A higher content of excess silicon in SiO_x films leads to deterioration of the functional characteristics. The oxygen vacancies and silicon dangling bonds, which are common defects found in SiO_x films lead to specific bound states for the electrons and holes and act as trap centers [27,35,36]. The memristor operation principle is based on the dielectric active medium switching between high-resistance and low-resistance logical states (HRS and LRS, respectively). In terms of the mechanism for switching the memristor between HRS and LRS, the filamentary model currently dominates. According to this model, the transition from a high-resistance to a low-resistance state occurs due to the formation of a filamentary path. In the LRS state, the memristor conductivity is determined by the charge-transporting capabilities of the filament. The excessive defects in the SiOx layer may create multiple conduction paths. To switch from LRS back to HRS, a negative voltage V_{reset} must be applied to rupture the conducting path. Although the conducting paths were ruptured, the charge carriers in the SiO_x layer, whose the short-range order obeys the RM model, had a high possibility to conduct current in parallel ways via hopping through nearby defects. This leads to a high value of the measured current in the HRS state during further cycling. By applying a positive voltage V_{set} to the upper electrode, conductive paths for transporting charge carriers can be formed again. However, in memristors, based on SiO_x, whose active layer obeys the RB model, the probability of the formation of such

additional channels is sharply reduced. This also affects the decrease of current in memristors with an active layer based on these films in the HRS. In the SiO_x layer, who's the short-range order obeys the RM model, the formation of a filament can occur not only due to oxygen vacancies, but also through the formation of Si dangling bonds around them. Therefore, with repeated switching from the HRS state to the LRS state and back, the film structure in the filament region will change irreversibly. And in order to return to the initial resistance in the HRS, it is necessary to apply a voltage much higher than the operating switching voltage. This leads to irreversible damage and destruction of the structure, as we observe in the experiment (see Fig. 2c). The excess silicon creates irreversible short-circuit conductive channels, which prevent the memristor from switching.

The very fact that the content of excess silicon in the non-stoichiometric Si-containing dielectric films exerts an influence on the memristor characteristics has been previously pointed out in the number of works [15,22,27,34,37]. The reasons for such an impact are also discussed here. However, no attention has been paid to the correlation between the short-range atomic order and the functional characteristics of resistive devices. We also note that similar correlation between the short-range atomic order and the characteristics of ReRAM devices was previously observed for SiO_xN_y films [25].

4. Conclusion

In conclusion, the reported results prove the correlation between the short-range order in the arrangement of atoms in non-stoichiometric SiO_x films and the functional parameters of the memristors (ReRAM) employing such films. Memristors (ReRAM) with an active layer whose microstructure exhibits a short-range order in the arrangement of atoms obeying the disordered Random Bonding (RB) model demonstrates the best set of characteristics. We believe that this result can be applied to all amorphous layers of non-stoichiometric silicon-containing dielectrics (SiO_x, SiN_y, and SiO_xN_y).

Funding and acknowledgments

The research was carried out within the state assignment of Ministry of Science and Higher Education of the Russian Federation (the theme No. FWGW-2022–0011 – the sample synthesis and electrical measurements, the theme No. FWGW-2022–0003 – the short-range order calculation). The use of the Center of Shared Facilities at MIPT for endurance test measurements is acknowledged. The authors (A.K. and A. Z.) are thankful to Islam Mutaev for his assistance in conducting endurance test measurements on memristor devices.

CRediT authorship contribution statement

G.N. Kamaev: Writing – review & editing, Writing – original draft, Visualization, Validation, Investigation, Conceptualization. **Yu.N. Novikov:** Writing – review & editing, Visualization, Methodology, Formal analysis. **I.P. Prosvirin:** Investigation, Formal analysis. **A.A. Gismatulin:** Writing – review & editing, Visualization, Investigation. **A. R. Khanas:** Investigation. **A.V. Zenkevich:** Writing – review & editing, Visualization, Validation, Resources. **V.A. Gritsenko:** Writing – review & editing, Supervision, Project administration, Methodology, Conceptualization.

Declaration of competing interest

The authors declare that they have no known competing financial interests or personal relationships that could have appeared to influence the work reported in this paper.

Data availability

Data will be made available on request.

References

[1] M.A. Zidan, J.P. Strachan, W.D. Lu, The future of electronics based on memristive systems, Nat. Electron. 1 (2018) 22–29, https://doi.org/10.1038/s41928-017-0006-8.
[2] B. Sun, S. Ranjan, G. Zhou, T. Guo, Y. Xia, L. Wei, Y.N. Zhou, Y.A. Wu, Multistate resistive switching behaviors for neuromorphic computing in memristor, Mater. Today Adv. 9 (2021) 100125, https://doi.org/10.1016/j.mtadv.2020.100125.
[3] Y. Shi, L. Nguyen, S. Oh, et al., Neuroinspired unsupervised learning and pruning with subquantum CBRAM arrays, Nat. Commun. 9 (2018) 5312, https://doi.org/10.1038/s41467-018-07682-0.
[4] C. Wang, G. Shi, F. Qiao, R. Lin, S. Wu, Z. Hu, Research progress in architecture and application of RRAM with computing-in-memory, Nanoscale Adv. 5 (2023) 1559–1573, https://doi.org/10.1039/D3NA00025G.
[5] X. Wang, F. Yang, Q. Liu, Z. Zhang, Z. Wen, J. Chen, Q. Zhang, C. Wang, G. Wang, F. Liu, Neuromorphic circuits based on memristors: endowing robots with a human-like brain, J. Semicond. 45 (2024) 061301.
[6] A. Mehonic, A. Sebastian, B. Rajendran, O. Simeone, E. Vasilaki, A.J. Kenyon, Memristors—from in-memory computing, deep learning acceleration, and spiking neural networks to the future of neuromorphic and bio-inspired computing, Adv. Intell. Syst. 2 (2020) 2000085, https://doi.org/10.1002/aisy.202000085.
[7] X. Zhang, A. Huang, Q. Hu, Z. Xiao, P.K. Chu, Neuromorphic computing with memristor crossbar, Phys. Status Solidi A 215 (2018) 1700875, https://doi.org/10.1002/pssa.201700875.
[8] S. Choi, T. Moon, G. Wang, et al., Filament-free memristors for computing, Nano Convergence. 10 (2023) 58, https://doi.org/10.1186/s40580-023-00407-0.
[9] J.H. Yoon, Y.-W. Song, W. Ham, J.-M. Park, J.-Y. Kwon, A review on device requirements of resistive random access memory (RRAM)-based neuromorphic computing, APL Mater. 11 (2023) 090701, https://doi.org/10.1063/5.0149393.
[10] H. Cao, H. Ren, A 10-nm-thick silicon oxide based high switching speed conductive bridging random access memory with ultra-low operation voltage and ultra-low LRS resistance, Appl. Phys. Lett. 120 (2022) 133502, https://doi.org/10.1063/5.0085045.
[11] S. Roy, E. Bhattacharya, B. Chakrabarti, Demonstration of a PECVD SiOx-based RRAM dendritic device, IEEE Electron Device Lett. 45 (2024) 364–367, https://doi.org/10.1109/LED.2023.3347333.
[12] A. Mehonic, A.L. Shluger, D. Gao, I. Valov, E. Miranda, D. Ielmini, A. Bricalli, E. Ambrosi, C. Li, J.J. Yang, Q. Xia, A.J. Kenyon, Silicon Oxide (SiO_x): a promising material for resistance switching? Adv. Mater. 30 (2018) 1801187 https://doi.org/10.1002/adma.201801187.
[13] A.A. Gismatulin, V.A. Voronkovskii, G.N. Kamaev, Y.N. Novikov, V.N. Kruchinin, G.K. Krivyakin, V.A. Gritsenko, I.P. Prosvirin, A. Chin, Electronic structure and charge transport mechanism in a forming-free SiO_x-based memristor, Nanotechnology 31 (2020) 505704, https://doi.org/10.1088/1361-6528/abb505.
[14] S. Kim, S. Jung, M.-H. Kim, Y.-C. Chen, Y.-F. Chang, K.-C. Ryoo, S. Cho, J.-H. Lee, B.-G. Park, Scaling effect on silicon nitride memristor with highly doped Si substrate, Small 14 (2018) 1704062, https://doi.org/10.1002/smll.201704062.
[15] T.X. Jiang, Z. Ma, J. Xu, K. Chen, L. Xu, W. Li, X. Huang, D. Feng, a-SiNx:H-based ultra-low power resistive random access memorywith tunable Si dangling bond conduction paths, Sci. Rep. 5 (2015) 15762, https://doi.org/10.1038/srep15762.
[16] A.A. Gismatulin, G.N. Kamaev, V.N. Kruchinin, V.A. Gritsenko, O.M. Orlov, A. Chin, Charge transport mechanism in the forming-free memristor based on silicon nitride, Sci. Rep. 11 (2021) 2417, https://doi.org/10.1038/s41598-021-82159-7.
[17] C. Li, L. Han, H. Jiang, et al., Three-dimensional crossbar arrays of self-rectifying Si/SiO_2/Si memristors, Nat. Commun. 8 (2017) 15666, https://doi.org/10.1038/ncomms15666.
[18] S. Kim, B.-G. Park, Nonlinear and multilevel resistive switching memory in Ni/Si_3N_4/Al_2O_3/TiN structures, Appl. Phys. Lett. 108 (2016) 212103, https://doi.org/10.1063/1.4952719.
[19] K. Leng, X. ZhuZ, X. Ma, J. Yu, L. Xu, W. Xu, K.C. Li, Artificial neurons and synapses based on Al/a-SiNxOy:H/P+ -Si device with tunable resistive switching from threshold to memory, Nanomaterials 12 (2022) 311, https://doi.org/10.3390/nano12030311.
[20] J.Y. Kwon, J.H. Park, T.G. Kim, Self-rectifying resistive-switching characteristics with ultralow operating currents in SiO_xN_y/AlN bilayer devices, Appl. Phys. Lett. 106 (2015) 223506, https://doi.org/10.1063/1.4922252.
[21] S. Kim, S. Jung, M.-H. Kim, S. Cho, B.-G. Park, Resistive switching characteristics of Si_3N_4-based resistive-switching random-access memory cell with tunnel barrier for high density integration and low-power applications, Appl. Phys. Lett. 106 (2015) 212106, https://doi.org/10.1063/1.4921926.
[22] H. Zhang, Z. Ma, X. Zhang, Y. Sun, J. Liu, L. Xu, W. Li, K. Chen, D. Feng, The ultra-low power performance of a-SiN_xO_y:H resistive switching memory, Phys. Status Solidi A 215 (2018) 1700753, https://doi.org/10.1002/pssa.201700753.
[23] I.P. Lisovskyy, M.V. Voitovich, A.V. Sarikov, V.G. Litovchenko, A.B. Romanyuk, V. P. Melnyk, I.M. Khatsevich, P.E. Shepeliavyi, Transformation of the structure of silicon oxide during the formation of Si nanoinclusitions under thermal annealings, Ukr. J. Phys. 54 (2009) 383–390.
[24] M. Molinari, H. Rinnert, M. Vergnat, Evolution with the annealing treatments of the photoluminescence mechanisms in a-SiN_x: H alloys prepared by reactive

evaporation, J. Appl. Phys. 101 (2007) 123532, https://doi.org/10.1063/1.2749283.
[25] Y.N. Novikov, G.N. Kamaev, I.P. Prosvirin, V.A. Gritsenko, Memory properties and short-range order in silicon oxynitride-based memristors, Appl. Phys. Lett. 122 (2023) 232903, https://doi.org/10.1063/5.0151211.
[26] T.V. Perevalov, V.A. Volodin, G.N. Kamaev, A.A. Gismatulin, S.G. Cherkova, I. P. Prosvirin, K.N. Astankova, V.A. Gritsenko, Electronic structure of silicon oxynitride films grown by plasma-enhanced chemical vapor deposition for memristor application, J. Non Cryst. Solids 598 (2022) 121925, https://doi.org/10.1016/j.jnoncrysol.2022.121925.
[27] F.G. Bell, L. Ley, Photoemission study of SiO (0&x (2) alloys, Phys. Rev. B. 37 (1988) 8383, https://doi.org/10.1103/PhysRevB.37.8383.
[28] Y.N. Novikov, V.A. Gritsenko, Short-range order in amorphous SiO_x by x ray photoelectron spectroscopy, J. Appl. Phys. 110 (2011) 014107, https://doi.org/10.1063/1.3606422.
[29] V.A. Gritsenko, Yu N. Novikov, A. Chin, Nanoscale potential fluctuations and electron percolation in silicon oxide (SiOx, x = 1.4, 1.6), Mater. Res. Express 6 (2019) 116409, https://doi.org/10.1088/2053-1591/ab448.
[30] M. Lanza, H.-S. Philip, E. Wong, D. Pop, D. Ielmini, B.C. Strukov, L. Regan, M. A. Larcher, J.J. Villena, L. Yang, A. Goux, Y. Belmonte, F.M. Yang, J. Puglisi, B. Kang, E. Magyari-Köpe, A. Yalon, M. Kenyon, A. Buckwell, A. Mehonic, H. Shluger, T.-H. Li, B. Hou, D. Hudec, R. Akinwande, S. Ge, J.B. Ambrogio, E. Roldan, J. Miranda, K.L. Suñe, X. Pey, N. Wu, E. Raghavan, W.D.L. Wu, G. Navarro, W. Zhang, H. Wu, R. Li, A. Holleitner, U. Wurstbauer, M.C. Lemme, M. Liu, S. Long, Q. Liu, H. Lv, A. Padovani, P. Pavan, I. Valov, X. Jing, T. Han, K. Zhu, S. Chen, F. Hui, Y. Shi, Recommended methods to study resistive switching devices, Adv. Electron. Mater. 5 (2018) 1800143, https://doi.org/10.1002/aelm.201800143.
[31] M. Lanza, R. Waser, D. Ielmini, J.J. Yang, L. Goux, J. Suñe, A.J. Kenyon, A. Mehonic, S. Spiga, V. Rana, S. Wiefels, S. Menzel, I. Valov, M.A. Villena, E. Miranda, X. Jing, F. Campabadal, M.B. Gonzalez, F. Aguirre, F. Palumbo, K. Zhu, J.B. Roldan, F.M. Puglisi, L. Larcher, T.-H. Hou, T. Prodromakis, Y. Yang, P. Huang, T. Wan, Y. Chai, K.L. Pey, N. Raghavan, S. Dueñas, T. Wang, Q. Xia, S. Pazos, Standards for the characterization of endurance in resistive switching devices, ACS Nano 15 (11) (2021) 17214–17231, https://doi.org/10.1021/acsnano.1c06980.
[32] K.M. Kim, J.J. Yang, J.P. Strachan, E.M. Grafals, N. Ge, N.D. Melendez, Z. Li, R. S. Williams, Voltage divider effect for the improvement of variability and endurance of TaOx memristor, Sci. Rep. 6 (2016) 20085, https://doi.org/10.1038/srep20085.
[33] V. Ravi, S.R.S. Prabaharan, Fault tolerant adaptive write schemes for improving endurance and reliability of memristor memories, Int. J. Electron. Commun. (AEÜ) 94 (2018) 392–406, https://doi.org/10.1016/j.aeue.2018.07.023.
[34] Y. Wang, X. Qian, K. Chen, Z. Fang, W. Li, J. Xu, Resistive switching mechanism in silicon highly rich SiO_x ($x < 0.75$) films based on silicon dangling bonds percolation model, Appl. Phys. Lett. 102 (2013) 042103, https://doi.org/10.1063/1.4776695.
[35] G. Pacchioni, G. Ierańo, Ab initio theory of optical transitions of point defects in SiO_2, Phys. Rev. B 57 (1998) 818, https://doi.org/10.1103/PhysRevB.57.818.
[36] A.-M. El-Sayed, M.B. Watkins, V.V. Afanas'ev, A.L. Shluger, Nature of intrinsic and extrinsic electron trapping in SiO_2, Phys. Rev. B 89 (2014) 125201, https://doi.org/10.1103/PhysRevB.89.125201.
[37] T.J. Yen, A. Chin, V.A. Gritsenko, High performance all nonmetal SiNx resistive random access memory with strong process dependence, Sci. Rep. 10 (2020) 2807, https://doi.org/10.1038/s41598-020-59838-y.